Regorafenib and Nifuroxazide exert enhanced suppression of hepatocellular carcinoma by inhibiting STAT3 and immune remodeling

KUN LI[1*], JINWEI CHEN[2*], ZHI ZHENG[1], YICHUN GAO[3], JIAYU ZHANG[3], WENYA DING[3], TONGGUO YANG[1], YUYANG GU[1], XUHUA DUAN[1], TIESUO ZHAO[1], HUIJIE JIA[1], PENGFEI CHEN[1,4] and JIANZHUANG REN[1]

[1]Department of Interventional Radiology, The First Affiliated Hospital of Zhengzhou University, Zhengzhou, Henan 450000, P.R. China; [2]Department of Radiology, Shanxi Cancer Hospital, Shanxi Medical University, Taiyuan, Shanxi 030000, P.R. China; [3]Xinxiang City Key Laboratory of Tumor Vaccine and Immunotherapy, Xinxiang Engineering Technology Research Center of Immune Checkpoint Drug for Liver-Intestinal Tumors, Henan Medical University, Xinxiang, Henan 453000, P.R. China; [4]Department of Radiology, The First Affiliated Hospital of Xi'an Jiaotong University, Xi'an, Shanxi 710000, P.R. China

Received July 30, 2025; Accepted January 5, 2026

DOI: 10.3892/or.2026.9074

Abstract. Regorafenib, a multi-kinase inhibitor, has limited efficacy in hepatocellular carcinoma (HCC) due to dose-dependent toxicity. The present study explored whether low-dose Regorafenib combined with Nifuroxazide exerts enhanced anti-tumor effects in HCC models. *In vitro* experiments with HepG2 cells showed the combination inhibited cell viability, proliferation and migration, induced apoptosis and reduced expression of key proteins, including phosphorylated signal transducer and activator of transcription 3 (STAT3). *In vivo*, H22 tumor-bearing mice treated with the combination exhibited suppressed tumor growth without systemic toxicity, along with changes in apoptotic proteins, enhanced tumor-infiltrating immune cells and improved systemic immune responses. These findings indicated that the combination exerts enhanced suppression of HCC by inhibiting STAT3 and remodeling anti-tumor immunity, providing preclinical evidence for a safe and effective strategy.

Correspondence to: Professor Jianzhuang Ren, Department of Interventional Radiology, The First Affiliated Hospital of Zhengzhou University, 1 Longhu Zhonghuan Road, Jinshui, Zhengzhou, Henan 450000, P.R. China
E-mail: fccrenjz@zzu.edu.cn

*Contributed equally

Abbreviations: HCC, hepatocellular carcinoma; JAK2, Janus kinase 2; p-JAK2, phosphorylated Janus kinase 2; STAT3, signal transducer and activator of transcription 3; PD-L1, programmed death ligand 1; SHP-1, Src homology region 2 domain-containing phosphatase 1; VEGF, vascular endothelial growth factor; CCK-8, Cell Counting Kit-8; TUNEL, terminal deoxynucleotidyl transferase dUTP nick end labeling; GO, Gene Ontology; KEGG, Kyoto Encyclopedia of Genes and Genomes; GSEA, Gene Set Enrichment Analysis

Key words: antineoplastic, angiogenesis inhibitors, hepatocellular carcinoma, immunotherapy, immune checkpoint inhibitors

Introduction

Primary liver cancer is the sixth most common cancer type worldwide and the third leading cause of cancer-related mortality (1). It is predicted that the number of new cases of liver cancer will increase by 55.0% between 2020 and 2040, with an estimated 1.4 million new cases of hepatocellular carcinoma (HCC) expected in 2040 (2). With its continuously increasing incidence and mortality rates, HCC imposes a significant and challenging health burden globally (3). However, most patients with HCC are diagnosed with intermediate or advanced stage cancer in the first instance and only 15-25% are eligible for curative resection (1). For patients with intermediate or advanced liver cancer, systemic therapies such as immunotherapy or targeted therapy are the preferred approaches (4).

Regorafenib, an oral multi-kinase inhibitor, can inhibit the activation of multiple target kinases, including rapidly accelerated fibrosarcoma (RAF), vascular endothelial growth factor receptor (VEGFR) and platelet-derived growth factor receptor (PDGFR). It functions by inhibiting angiogenesis and tumor cell proliferation and has become a cornerstone of second-line therapy for the management of advanced HCC (5,6). Several clinical trials have evaluated Regorafenib in patients with previously treated HCC. The REACHIN and RESORCE trials demonstrated significant improvements in progression-free survival (PFS) and tumor control benefits with Regorafenib in second or third-line settings (7,8). However, its clinical application is still plagued by multiple challenges: The REACHIN, RESORCE and CORRECT trials showed that the use at the recommended dose (160 mg daily) is often limited by prominent treatment-related adverse events, including hand-foot skin reactions, diarrhea and hypertension, among other adverse events (7-9). In a clinical trial of Regorafenib combined

with nivolumab, the combination of 80 mg Regorafenib with nivolumab showed improved safety and effective anti-tumor activity in previously treated patients with advanced gastric or colorectal cancer (10). More importantly, the immunomodulatory effects of Regorafenib are dose-dependent: High doses may induce a hypoxic tumor microenvironment, recruit immunosuppressive cells such as tumor-associated macrophages (TAMs) and thereby exacerbate immune evasion (11). By contrast, low doses can promote favorable macrophage polarization and boost T cell activity. Researchers have demonstrated that a low concentration of Regorafenib, combined with JAK/HDAC small-molecule inhibitors or anti-PD-1 therapy, exerts synergistic anti-tumor efficacy with higher Regorafenib bioavailability (10,12). These observations strongly suggest that the optimal immunomodulatory dose of Regorafenib may be lower than the recommended monotherapy dose, underscoring the need for combination therapy.

STAT3 is a member of the signal transducer and activator of transcription (STAT) family. In response to cytokines and growth factors, STAT3 is phosphorylated and mediates the expression of various genes. Sustained activation of STAT3 can induce cancer through multiple mechanisms, including reducing tumor cell apoptosis, increasing tumor cell proliferation, promoting tumor angiogenesis and regulating tumor immune evasion (13). Nifuroxazide is a nitrofuran derivative with broad-spectrum antibacterial activity (14). Nifuroxazide can reduce the viability of various cancer cells by inhibiting STAT3 phosphorylation (15). More importantly, Nifuroxazide can inhibit programmed death ligand 1 (PD-L1) expression in HCC, promote T cell activation and enhance anti-tumor immune responses (16,17). Ye *et al* (18) also found that Nifuroxazide reduced the number of myeloid-derived suppressor cells and M2-type macrophages in tumors, exerting a positive effect on the tumor immune microenvironment. However, tumor progression is extremely complex and the efficacy of single-agent therapy is limited, necessitating more aggressive treatment strategies.

Therefore, the present study was performed to evaluate the efficacy of Regorafenib combined with Nifuroxazide and to determine whether this combination therapy enhanced the therapeutic effects. In the present study, the role of this combination in enhancing therapeutic efficacy was assessed using *in vitro* and *in vivo* preclinical HCC models. It was found that Regorafenib combined with Nifuroxazide exerted enhanced anti-angiogenic effects, promoted tumor cell apoptosis and inhibited the proliferation and migration of HCC cells. Additionally, low-dose Regorafenib promoted immune cell infiltration and polarized macrophages toward an M1 phenotype, thereby enhancing cytotoxic T cell functions and anti-tumor immunity, with the combination therapy showing further enhanced effects.

Materials and methods

Reagents and cell lines. Human HepG2 cells and the mouse H22 hepatoma cells were obtained from Professor Xuejian Zhao (Department of Pathophysiology, Prostate Diseases Prevention and Treatment Research Centre, Norman Bethune College of Medicine, Jilin University, Changchun, China). All cell lines used in the present study have been authenticated to ensure identity and purity. Human HepG2 cells were authenticated by short tandem repeat (STR) profiling, which matched the reference STR data of ATCC HB-8065. Mouse H22 hepatoma cells were verified by morphological observation and functional validation (consistent tumorigenicity in C57BL/6 mice). The two cell lines were tested negative for mycoplasma contamination using a mycoplasma detection kit (Beyotime Biotechnology; cat. no. C0301). HepG2 cells, which were initially reported as a hepatoma cell line in early studies (19) but subsequently classified as a hepatoblastoma cell line (20,21), are widely used in liver cancer research. HepG2 cells were cultured in high-glucose DMEM (Thermo Fisher Scientific Inc.) with 1% penicillin-streptomycin and 10% FBS (Sunrise Material Co., Ltd.) at 37˚C in a humidified atmosphere containing 5% CO_2. H22 cells were expanded via ascites in C57BL/6 mice (Henan Skobes Biotechnology Co., Ltd.). Nifuroxazide (MilliporeSigma) and Regorafenib (Bayer AG) were used in the present study; the therapeutic doses of Nifuroxazide used were based on previous studies for maximal therapeutic benefit (10 μg/ml in HepG2 and 10 mg/kg/day in mouse models) (16,18). Regorafenib doses (5 μg/ml in HepG2 cells and 5 mg/kg/day in mouse models) were lower than clinical recommendations, but were based on a previous study (10).

Cell viability assay. HepG2 cells were seeded at a density of $1x10^4$ cells/well in 96-well plates (Corning, Inc.) and cultured in high-glucose DMEM supplemented with 10% FBS and 1% penicillin-streptomycin at 37˚C in a humidified atmosphere containing 5% CO_2 for 16 h, after which Regorafenib and Nifuroxazide were added. After 24 h of treatment, 10 μl CCK-8 solution (Beyotime Biotechnology) was added and cells were incubated for a further 2 h. Optical density was measured at 450 nm using a microplate reader (SpectraMax iD3; Molecular Devices, LLC).

Wound healing assay. HepG2 cells were seeded at a density of $3.5x10^5$ cells/well in six-well plates and cultured for 16 h at 37˚C. The cells were then serum-starved (no FBS) for 24 h at 37˚C. Scratches were created in the center of each well using a 200 μl pipette tip, then Regorafenib (5 μg/ml) and Nifuroxazide (10 μg/ml) were added. After 24 and 48 h, scratch widths were measured and recorded using a light microscope (Nikon Corporation). For quantification, scratch widths were analyzed via ImageJ software (version 1.54f; National Institutes of Health); wound healing rate=(Initial scratch width-width at 24/48 h)/Initial scratch width x100%, normalized wound healing rate=(wound healing rate of each group/average wound healing rate of the control group), and each sample was measured in ≥3 random fields with mean values for statistical analysis.

Colony formation assay. HepG2 cells were seeded at a density of $2x10^3$ cells/well in six-well plates and cultured for 14-16 h at 37˚C, after which Regorafenib (5 μg/ml) and Nifuroxazide (10 μg/ml) were added. The media was replaced periodically. Cell colonies visible to the naked eye appeared on day 10, at which point, they were measured and recorded.

Apoptosis assay. Apoptosis was assessed using an Annexin V-FITC kit. HepG2 cells were seeded at a density of

$3.5x10^5$ cells/well in six-well plates and cultured for 14-16 h at 37˚C. Regorafenib (5 μg/ml) and Nifuroxazide (10 μg/ml) were added and cells were incubated for 24 or 48 h at 37˚C. Cells were harvested, stained with Annexin V-FITC and PI (Dojindo Laboratories, Inc.) at room temperature (25±2˚C) in the dark for 15 min, resuspended in 400 μl PBS and analyzed using a flow cytometer (Beckman Coulter, Inc.) with analysis performed using CytExpert Software (version 2.1; Beckman Coulter, Inc.) and the apoptotic rate calculated as the sum of the percentage of early apoptotic cells and late apoptotic cells.

Establishment of a mouse HCC model. Female C57BL/6 mice (6-8 weeks old, weighing 16-20 g, n=24) were obtained from Henan Skobes Biotechnology Co., Ltd. Female mice were selected because they exhibit more stable metabolism, stronger resistance to diet-induced obesity and metabolic imbalances, higher leptin sensitivity and compensatory hypothalamic Pomc mRNA expression, all reducing experimental variability and ensuring reliable tumorigenicity of H22 cells (22). Mice were housed in a specific pathogen-free grade animal room with individually ventilated cages at 24±2˚C, at 40-50% humidity, with a 12-h light/dark cycle and *ad libitum* access to sterile food/water. H22 cells ($2x10^6$ cells/100 μl) were subcutaneously injected into the right dorsal side of mice. To minimize animal suffering, humane endpoints were set: Tumor volume ≤2,000 mm^3, >20% initial weight loss in 3 consecutive days, or severe distress (such as labored breathing, inability to access food/water); mice meeting any endpoint were sacrificed immediately. All mice were sacrificed in accordance with the preset experimental protocol at the end of the study.

A total of 7 days post-injection, mice were randomly divided into four groups (n=6 per group): PBS group (daily gavage of 100 μl PBS); Regorafenib group (daily gavage, 5 mg/kg); Nifuroxazide group (daily gavage, 10 mg/kg); combination group (daily Regorafenib gavage 5 mg/kg + Nifuroxazide gavage 10 mg/kg). Treatments were administered daily for 7 days. Mice were sacrificed via intraperitoneal injection of 2% tribromoethanol (20 ml/kg, deep anesthesia confirmed by absent pedal reflex) followed by overdose sodium pentobarbital (150 mg/kg) 1 day after completion of the treatment regimen. Mortality was confirmed by cessation of respiration/heartbeat, absent corneal reflex and persistent muscle flaccidity. Subsequently, tumor tissues were excised, weighed and images captured. All procedures were approved by the Animal Ethics Committee of the First Affiliated Hospital of Zhengzhou University (approval no. 2023-KY-1333) and adhered to the international 3R Principles (replacement, reduction, refinement).

Flow cytometry. Spleen and peripheral blood cell suspensions were prepared and treated with red blood cell lysis buffer (Beyotime Biotechnology) to remove red cells. Cell density was adjusted to $1x10^7$ cells/ml. A total of 100 μl suspension per sample was stained with fluorescently-labeled antibodies against CD3 (BioLegend, Inc.; cat. no. 100204; 1:200), CD4 (BioLegend, Inc.; cat. no. 100406; 1:200), CD8 (BioLegend, Inc.; cat. no. 100706; 1:200), CD45 (BD Biosciences; cat. no. 553080; 1:200), CD11b (BioLegend, Inc.; cat. no. 101206; 1:200), CD206 (BioLegend, Inc.; cat. no. 141708; 1:200), CD86 (BioLegend, Inc.; cat. no. 105006; 1:200), or F4/80 (BioLegend, Inc.; cat. no. 123116; 1:200) according to the manufacturer's protocol. Samples were stained with the aforementioned fluorescently-labeled antibodies incubated in the dark at 4˚C for 30 min, washed with pre-cooled PBS three times and resuspended in 400 μl PBS. The fluorescence intensity was measured using a CytoFLEX flow cytometer (Beckman Coulter, Inc.).

Western blotting. Proteins were extracted using RIPA lysis buffer (Beyotime Biotechnology, cat. no. P0013B) supplemented with 1% protease inhibitor cocktail and 1% phosphatase inhibitor cocktail. Protein concentration was determined via the BCA Protein Assay Kit (Beyotime Biotechnology; cat. no. P0010) following the manufacturer's protocol. A total of 10 μg protein per lane was separated via SDS-PAGE using 10% Tris-Gly SDS-PAGE precast gels (Beyotime Biotechnology; cat. no. P0052A), followed by transfer to PVDF membranes (MilliporeSigma) at 220 mA. Membranes were blocked with 5% skimmed milk in 0.05% Tween-20 at room temperature for 1 h, then incubated overnight at 4˚C with one of the following primary antibodies: anti-PD-L1 (1:1,000; Shanghai Abways Biotechnology Co., Ltd.; cat. no. CY5980); anti-VEGF (1:2,000, Affinity Biosciences, Ltd.; cat. no. AF5131); anti-p-STAT3 (1:1,000, Cell Signaling Technology, Inc.; cat. no. 9145); anti-STAT3 (1:1,000, Cell Signaling Technology, Inc.; cat. no. 9139); anti-Bcl-2 (1:2,000, Shanghai Abways Biotechnology Co., Ltd.; cat. no. CY6717); anti-Bax (1:2,000, Shanghai Abways Biotechnology Co., Ltd.; cat. no. CY5059); anti-MMP2 (1:1,000, Cell Signaling Technology, Inc.; cat. no. 40994); anti-cyclin D1 (1:2,000, Santa Cruz Biotechnology, Inc.; cat. no. sc-8396); anti-cleaved-caspase 3 (1:2,000, Cell Signaling Technology; cat. no. 9664); anti-caspase 3 (1:2,000, Cell Signaling Technology; cat. no. 9662); phospho-JAK2 (1:1,000; UpingBio technology Co, Ltd.; cat. no. YP-Ab-14423); JAK2 (1:1,000; UpingBio technology Co, Ltd.; cat. no. YP-Ab-14800); SHP-1 (1:1,000; UpingBio technology Co, Ltd.; cat. no. YP-mAb-14236); anti-Tubulin (1:4,000, MilliporeSigma; cat. no. T9026); and anti-GAPDH (1:4,000, MilliporeSigma; cat. no. G8795) according to the manufacturer's protocol. Following washing, membranes were incubated with a horseradish peroxidase (HRP)-conjugated secondary antibody (1:5,000; OriGene Technologies, Inc.; cat. nos. TA373082/TA373083) at room temperature for 60 min. Signals were visualized using an enhanced chemiluminescence kit (Beyotime Biotechnology; cat. no. P0018) and imaged using a Fusion FX spectra imaging system (Vilber Lourmat). Densitometric analysis was performed using ImageJ software (version 1.54f; National Institutes of Health, USA).

Immunofluorescence imaging. Immunofluorescence imaging was used to detect $CD4^+$ and $CD8^+$ T cells and macrophage infiltration in tumor tissues. Tumor sections were prepared as follows: Freshly excised tumor tissues were fixed in 4% paraformaldehyde (room temperature, 4-6 h), rinsed with PBS (Beyotime Biotechnology), then dehydrated via gradient ethanol and transparentized with xylene. Tissues were embedded in paraffin (56-58˚C), sectioned into 4-μm slices

with a rotary microtome, mounted on poly-L-lysine-coated slides and baked at 60˚C for 2-3 h to secure slices. Prior to primary antibody incubation, the prepared tumor sections were dewaxed, rehydrated through a reversed graded ethanol series, and rinsed thoroughly with PBS. Sections were then blocked with 5% normal goat serum (Beyotime Biotechnology, cat. no. C0265) for 30 min at room temperature to eliminate non-specific antibody binding. The prepared tumor sections were incubated with the following primary antibodies: anti-CD3 (1:200; OmnimAbs; cat. no. OM244830); anti-CD4 (1:200; Cell Signaling Technology, Inc.; cat. no. 25229); anti-CD8 (1:400; Cell Signaling Technology, Inc.; cat. no. 98941); anti-CD206 (1:800; Cell Signaling Technology, Inc.; cat. no. 24595S); anti-CD86 (1:200, Novus Biologicals LLC; cat. no. NBP2-25208); or anti-Ki67 (1:100, Bioworld Technology, Inc.; cat. no. BS90769) according to the manufacturer's protocol, overnight at 4˚C. After washing with PBS, sections were incubated with the fluorescent-tagged secondary antibody (1:200; Shanghai Abways Biotechnology Co., Ltd.; cat. no. CY3101) for 30 min at room temperature. Following DAPI (Beyotime Biotechnology) staining at room temperature (25±2˚C) for 5 min and washing with PBS, slides were mounted using an anti-fade solution, visualized and imaged using a confocal microscope (AR1; Nikon Corporation) using a x20 objective lens.

TUNEL assay. Apoptosis in tissues was assessed using a TUNEL assay kit (Beyotime Biotechnology). Tumor sections were prepared, treated with DNase-free Proteinase K, incubated at 37˚C for 20 min, washed with PBS and treated with TUNEL solution at 37˚C for 60 min. Following DAPI (Beyotime Biotechnology) counterstaining at room temperature (25±2˚C) for 5 min and washing with PBS, slides were mounted using an anti-fade solution, visualized and imaged using a confocal microscope (AR1; Nikon Corporation) using a x20 objective lens.

Clustering and Gene Set Enrichment Analysis (GSEA). All analyzed datasets were retrieved from the Gene Expression Omnibus (GEO) database (https://www.ncbi.nlm.nih.gov/) under the accession number GSE148947 (10). RNA-seq data were processed using R software (version 4.1.0, https://www.r-project.org/), with the DESeq2, limma and clusterProfiler packages employed to identify differential gene expression (DGE) and perform Gene Ontology (GO), Kyoto Encyclopedia of Genes and Genomes (KEGG) and Gene Set Enrichment Analysis (GSEA). Gene sets for GSEA were obtained from the Molecular Signatures Database (https://www.gsea-msigdb.org/gsea/msigdb) (23) and no custom (unique) gene sets were applied in the analysis.

Statistical analysis. All experimental data were statistically analyzed using SPSS 24.0 software (IBM Corp.) and GraphPad Prism 8 software (Dotmatics). Results are presented as the mean ± standard deviation (SD), with each experiment was repeated independently at least three times to ensure reproducibility. Differences between multiple groups were assessed using one-way analysis of variance (ANOVA) followed by Tukey's HSD post hoc test. $P<0.05$ was considered to indicate a statistically significant difference.

Results

Transcriptome and functional analyses of the effects of Regorafenib and Nifuroxazide in HCC. Transcriptome profiling of Regorafenib-treated HCC cells ($P<0.05$, $\log_2FC >1$) revealed differential regulation of key genes; the results are shown as a heatmap (Fig. 1A), with GSEA (Fig. 1B) identifying immune pathway enrichment and inhibitory IL6-JAK-STAT3 signaling (Fig. 1C), indicative of STAT3-mediated immune remodeling. Kyoto Encyclopedia of Genes and Genomes (KEGG) and Gene Ontology (GO) enrichment analyses (Fig. S1) further delineated the following functional implications: Upregulated differentially expressed genes (DEGs) were clustered in immune-trafficking pathways (Fig. S1C) and GO terms for suppressed cell motility (Fig. S1D), while downregulated DEGs were associated with metabolic reprogramming (Fig. S1E and F). *In vitro*, CCK-8 (Fig. 1D and E) and colony formation assays (Fig. 1F and G) showed reduced proliferation and colony formation in HepG2 cells when treated with a combination of Regorafenib and Nifuroxazide, while wound-healing assays (Fig. 1H and I) showed the combination group exhibited reduced migration at both 24 and 48 h.

Effects of Nifuroxazide combined with Regorafenib on apoptosis in HepG2 cells. To clarify the pro-apoptotic effect and molecular mechanism of combination therapy, flow cytometry showed that monotherapy with Nifuroxazide and Regorafenib markedly induced HepG2 apoptosis and the apoptotic rate was further increased with combination treatment (Fig. 2A and B). Western blot analysis confirmed that both drugs reduced p-STAT3 expression, consistent with the IL6-JAK-STAT3 pathway inhibition based on GSEA and MMP2 expression and this reduction was more prominent in the combination treatment group (Fig. 2C and D; the original uncropped western blot images for the detections in this section are in Fig. S2). The present study further detected key molecules in the JAK2/SHP-1/STAT3 pathway: Compared with the control group, monotherapy with either drug markedly downregulated the expression of p-JAK2 and upregulated SHP-1 expression, while total JAK2 expression remained unchanged across all groups. The combination group exhibited a more pronounced downregulation of p-JAK2 and upregulation of SHP-1, which further supports the targeted inhibition of the STAT3 pathway by the combination therapy (Fig. S3A-D). Monotherapy with both drugs increased the expression of pro-apoptotic proteins (BAX and cleaved caspase-3) and decreased the expression of anti-apoptotic proteins (Bcl-2 and proliferation-related Cyclin-D1) and this effect was more pronounced in the combination group (Fig. 2C and D), indicative of increased apoptosis via the mitochondrial pathway. Additionally, monotherapy and combination therapy markedly reduced immune checkpoint PD-L1 and pro-angiogenic VEGF expression (both key in an immunosuppressive microenvironment), with a greater degree of downregulation in the combination group (Fig. 2C and D), a finding that was consistent with the findings of the transcriptomic analysis and GSEA results showing modulation of immune activation/anti-angiogenic regulatory characteristics.

Effect of Nifuroxazide combined with Regorafenib on tumor growth in a mouse model of HCC. At seven days after model

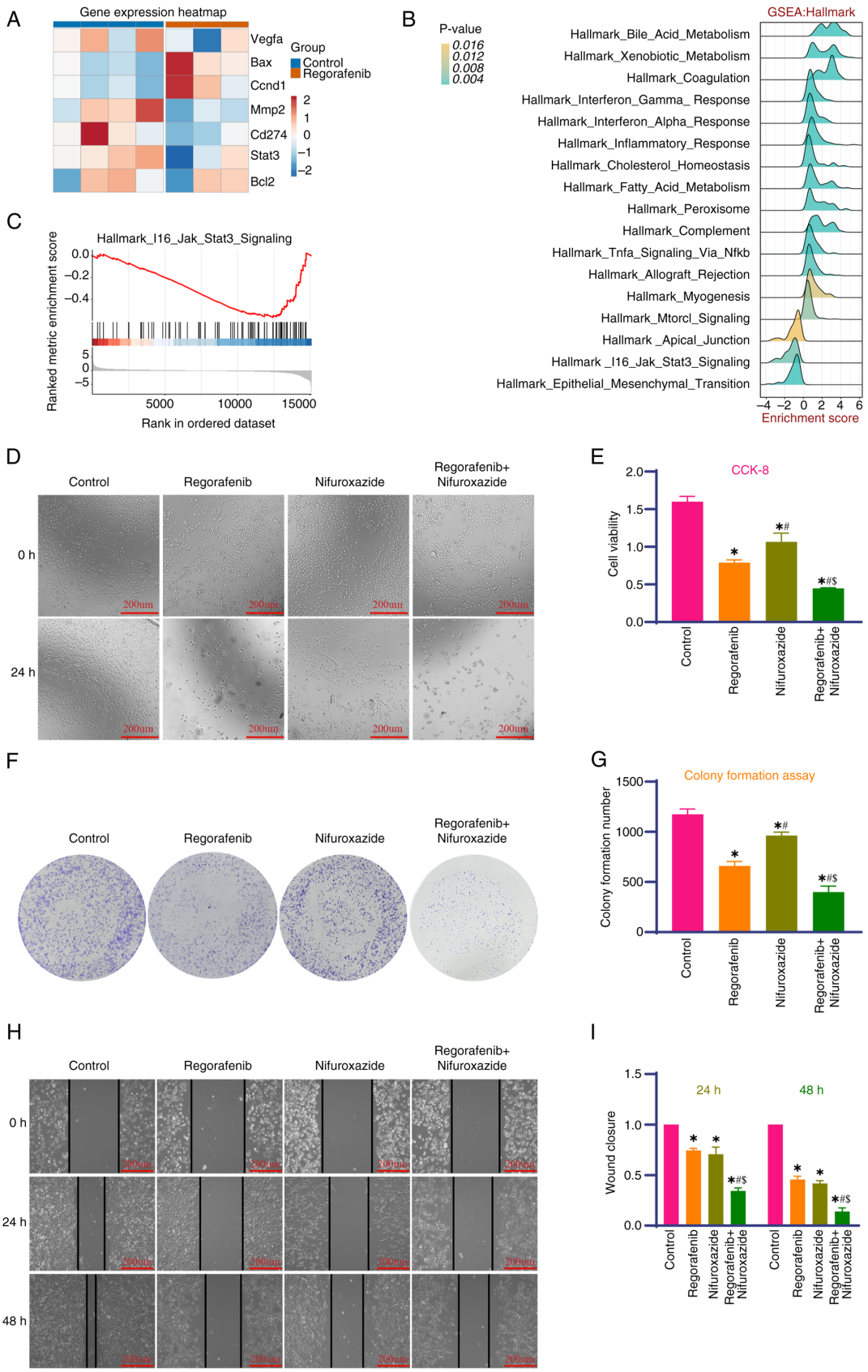

Figure 1. Transcriptome analysis reveals the mechanisms underlying the enhanced efficacy of Regorafenib and Nifuroxazide in HCC. (A) Gene expression heatmap of key genes (including Vegfa, Bax and STAT3) in Regorafenib-treated compared with control HCC cells. (B) GSEA-based enrichment of Hallmark pathways in Regorafenib-treated HCC cells. (C) GSEA enrichment plot for the Hallmark_IL6_Jak_STAT3_Signaling pathway. (D) Representative results of the CCK-8 assay (for cell viability) of HepG2 cells under different treatments. (E) Statistical analysis of cell viability in Fig. 1D. (F) Representative colony formation assay images of HepG2 cells under different treatments. (G) Statistical analysis of the number of colonies in Fig. 1F. (H) Representative wound-healing assay images (0, 24 and 48 h) of HepG2 cells under different treatments. (I) Statistical analysis of wound closure rate in Fig. 1H. Data are presented as mean ± standard deviation (n=3). *P<0.05 vs. the Control group; #P<0.05 vs. the Regorafenib group; $P<0.05 vs. the Nifuroxazide group. HCC, hepatocellular carcinoma; GSEA, Gene Set Enrichment Analysis.

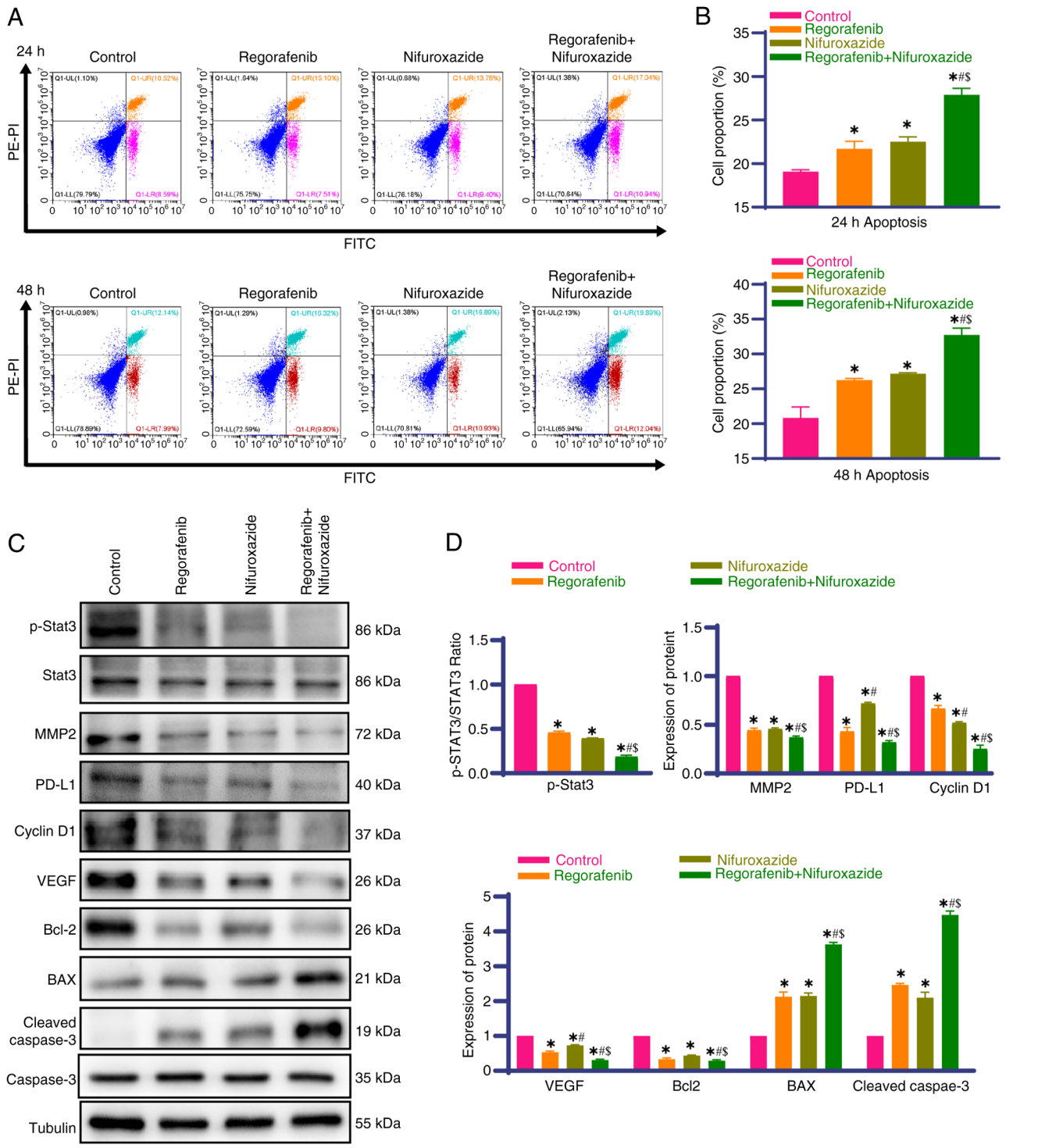

Figure 2. Effects of different treatments on apoptosis and the expression of related proteins. (A) Effects of Nifuroxazide combined with Regorafenib on HepG2 cell apoptosis detected by flow cytometry. (B) Statistical analysis of Fig. 2A. (C) Expression of related proteins in cells detected by western blotting. (D) Statistical analysis of Fig. 2C. Data are presented as mean ± standard deviation (n=3). *P<0.05 vs. the Control group; #P<0.05 vs. the Regorafenib group; $P<0.05 vs. the Nifuroxazide group. STAT3, signal transducer and activator of transcription 3; PD-L1, programmed death ligand 1; VEGF, vascular endothelial growth factor; p-, phosphorylated.

establishment, mice underwent 7 consecutive days of treatment. One day post-treatment, mice were sacrificed and tumor tissues were excised, weighed and images captured (Fig. 3A). The results showed that monotherapy with Nifuroxazide or Regorafenib markedly inhibited tumor growth compared with the PBS group and the combination group showed the greatest reduction in tumor growth (Fig. 3B-D). Body weight monitoring revealed no significant group differences despite variations in tumor volumes (Fig. 3E), suggesting no obvious systemic toxicity from the combination treatment.

Effects of Nifuroxazide and Regorafenib on apoptosis, proliferation, migration and PDL1 and VEGF expression in the mouse model of HCC. Tumor tissues were isolated for

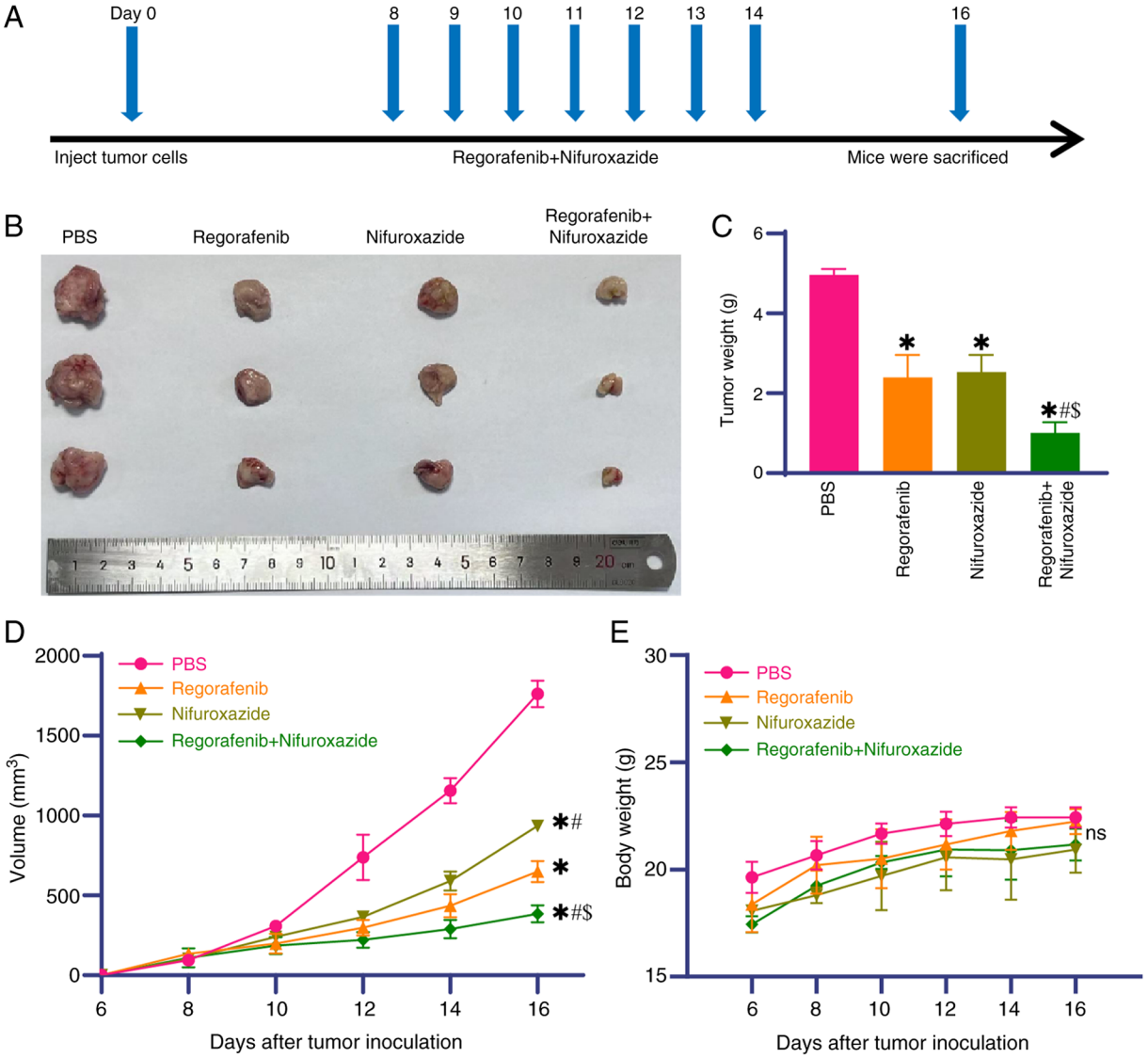

Figure 3. Effects of different treatments on tumor growth. (A) Treatment schedule: Mice were divided into four groups; each mouse subcutaneously inoculated with $1x10^6$ H22 cells prior to treatment. (B) Representative tumor images of each group. (C) Statistical analysis of tumor weight from Fig. 3B. (D) Statistical analysis of changes in tumor volume in mice. (E) Statistical analysis of changes in mouse body weight. Data are presented as mean ± standard deviation (n=6). *P<0.05 vs. the Control group; #P<0.05 vs. the Regorafenib group; $P<0.05 vs. the Nifuroxazide group.

detection 1 day after the final treatment. Western blotting showed that Nifuroxazide and Regorafenib monotherapy reduced p-STAT3 and MMP2 expression compared with the PBS group and the reductions in both were more pronounced in the combination group (Fig. 4A and B; the original uncropped western blot gel images for the related protein detections are Fig. S4). Consistent with the *in vitro* results, similar changes in the JAK2/SHP-1/STAT3 pathway were detected in tumor tissues: Compared with the PBS group, monotherapy groups showed markedly decreased p-JAK2 expression and increased SHP-1 expression, while total JAK2 levels were unchanged. The combination group had the most marked p-JAK2 down-regulation and SHP-1 upregulation, confirming the *in vivo* targeting of the STAT3 pathway by the combination therapy (Fig. S2E-H). Monotherapy with each drug upregulated the expression of pro-apoptotic BAX and cleaved-caspase-3, whilst downregulating the expression of anti-apoptotic Bcl-2 and proliferation-related CyclinD1, with a pronounced effect in the combination group (Fig. 4A and B). Similarly, mono-therapy with either drug reduced PD-L1 and VEGF expression and the effect was more pronounced in the combination group (Fig. 4A and B), consistent with the *in vitro* experiments and transcriptomic results. Immunofluorescence analysis showed lower Ki-67 expression (associated with proliferation) when treated with either drug alone compared with the PBS group and the decrease in expression was larger in the combination group (Fig. 4C and E). TUNEL assays showed fewer apoptotic cells in the PBS group, increased apoptosis in the monotherapy groups (either drug) and the highest number of apoptotic cells in the combination group (Fig. 4D and F). These results suggested that the combination treatment enhanced the anti-tumor effects of each drug *in vivo* by enhancing apoptosis and inhibiting proliferation/migration.

Nifuroxazide combined with regorafenib promotes the activation of tumor-infiltrating lymphocytes. To investigate the

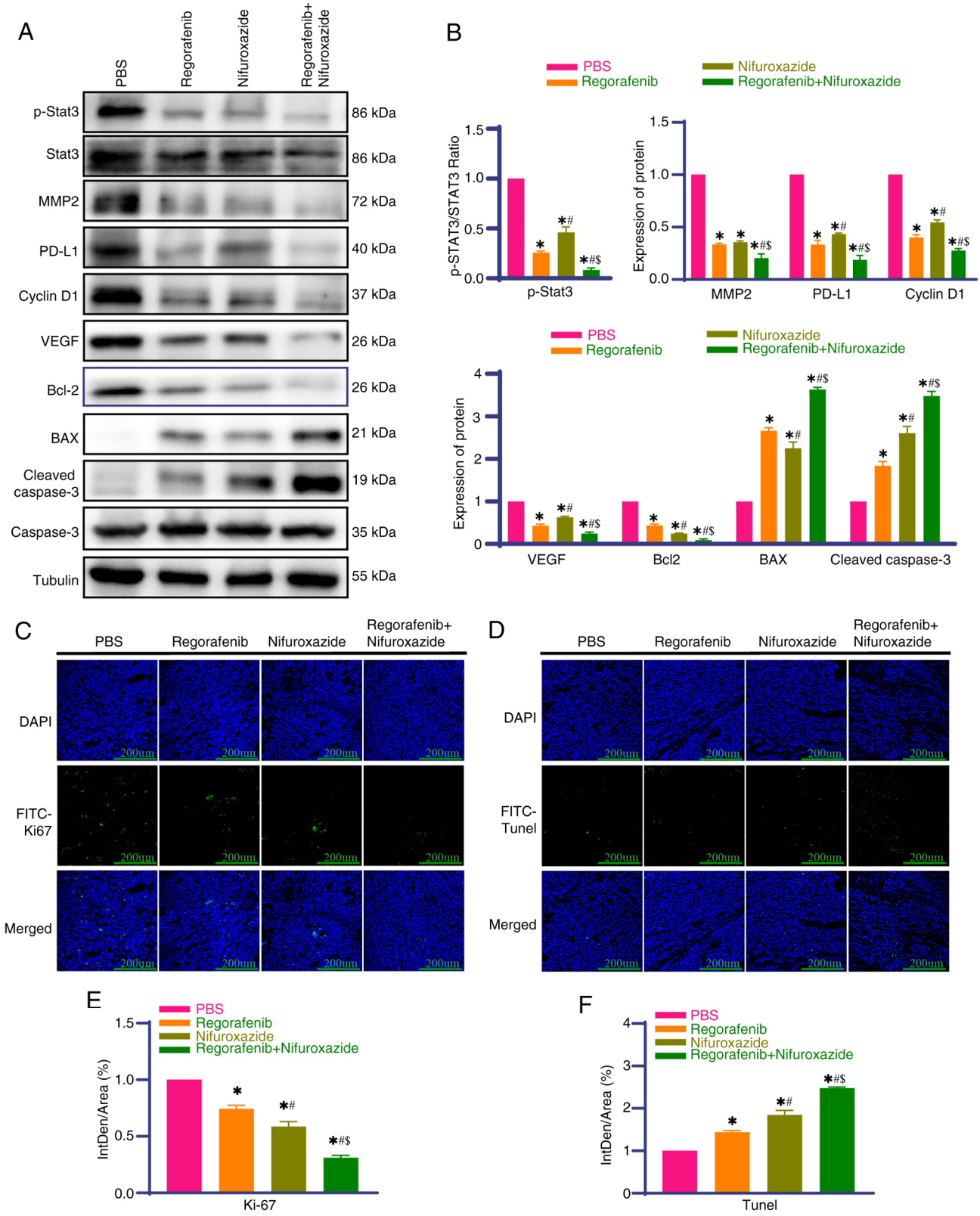

Figure 4. Effects of different treatments on cell apoptosis, proliferation, migration and the expression of related proteins. (A) Expression of related proteins detected by western blotting. (B) Statistical analysis of Fig. 4A. (C) Expression of Ki-67 in tumor tissues detected by immunofluorescence. (D) Tumor cell apoptosis in tumor tissues detected by TUNEL assay. (E) Statistical analysis of Fig. 4C. (F) Statistical analysis of Fig. 4D. Data are presented as mean ± standard deviation (n=3). *P<0.05 vs. the Control group; $^{\#}$P<0.05 vs. the Regorafenib group; $^{\$}$P<0.05 vs. the Nifuroxazide group. TUNEL, terminal deoxynucleotidyl transferase dUTP nick end labelling; STAT3, signal transducer and activator of transcription 3; PD-L1, programmed death ligand 1; VEGF, vascular endothelial growth factor; p-, phosphorylated.

effects of combination therapy on the tumor immune microenvironment, immunofluorescence was used to detect immune cell infiltration in tumor tissues. The results showed that compared with the PBS group, the monotherapy groups

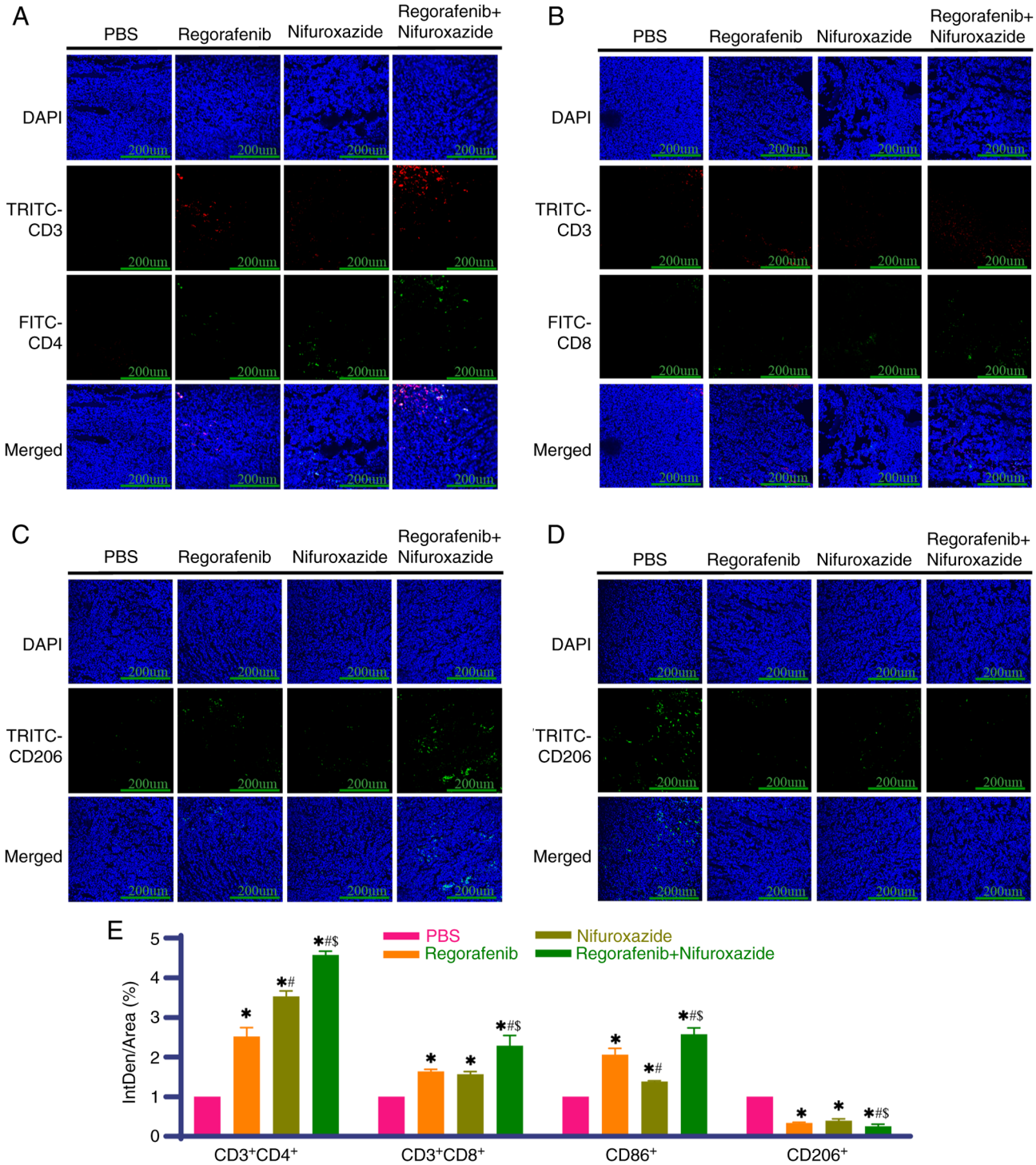

Figure 5. Effects of various treatments on immune cells in tumor tissues. (A-D) The expression of $CD3^+CD4^+$ T cells, $CD3^+CD8^+$ T cells, $CD86^+$ macrophages and $CD206^+$ macrophages in mouse tumor tissues. (E) Statistical analysis of Fig. 5A-D. Data are presented as mean ± standard deviation (n=3). *P<0.05 vs. the Control group; #P<0.05 vs. the Regorafenib group; $P<0.05 vs. the Nifuroxazide group.

exhibited markedly increased proportions of $CD3^+CD4^+$ and $CD3^+CD8^+$ T cells in tumor tissues and the increase was even higher in the combination group (Fig. 5A, B and E). Monotherapy with either drug increased the proportion of M1 macrophages and decreased the proportion of M2 macrophages, with a more pronounced effect in the combination group (Fig. 5C-E). Notably, activation of the PD-1/PD-L1 pathway impairs anti-tumor immunity by inhibiting T lymphocyte function and mediating tumor immune escape. Therefore, the results of the present study suggested that the combination treatment activated anti-tumor immunity and abrogated immune escape by promoting effector T cell infiltration and regulating macrophages toward a pro-inflammatory phenotype.

Nifuroxazide combined with regorafenib regulates the proportion of immune cells in the spleen and peripheral blood. The spleen, a core peripheral immune organ, is key

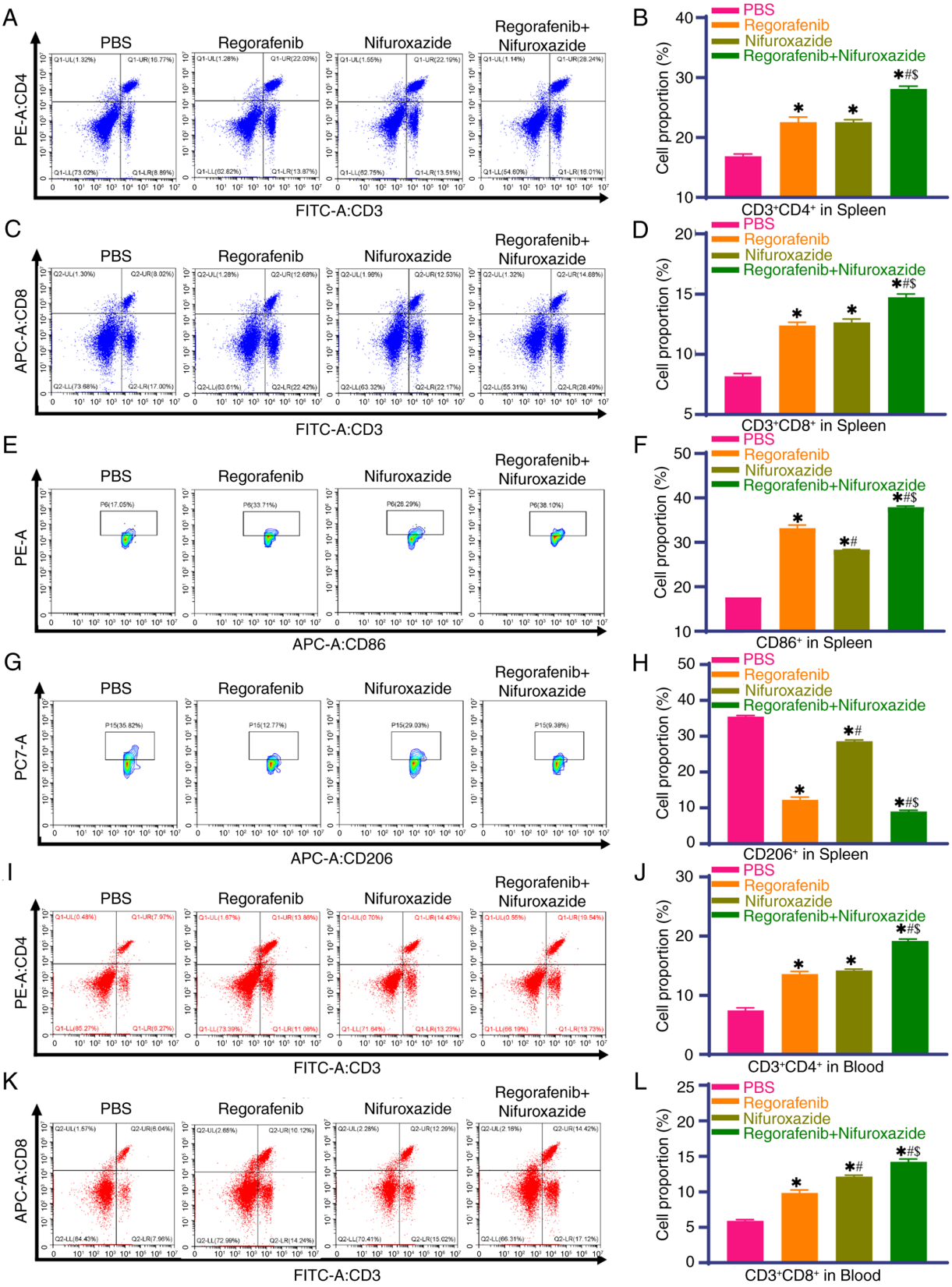

Figure 6. Effects of different treatments on immune cells. (A-H) Distribution and statistical analysis of $CD3^+CD4^+$ T cells, $CD3^+CD8^+$ T cells, $CD86^+$ cells and $CD206^+$ cells in mouse spleens. (I-L) Distribution and statistical analysis of $CD3^+CD4^+$ T cells and $CD3^+CD8^+$ T cells in peripheral blood. Data are presented as mean ± standard deviation (n=3). $^*P<0.05$ vs. the Control group; $^\#P<0.05$ vs. the Regorafenib group; $^\$P<0.05$ vs. the Nifuroxazide group.

in systemic immune responses. Flow cytometry showed that compared with the PBS group, Nifuroxazide and Regorafenib monotherapy groups had markedly higher proportions of splenic $CD3^+CD4^+$ T lymphocytes, $CD3^+CD8^+$ T lymphocytes and $CD86^+$ cells and lower $CD206^+$ cells and this effect was more prominent in the combination group (Fig. 6A-H). Further

analysis of peripheral blood circulating T lymphocytes revealed that the monotherapy and combination groups had a markedly higher proportion of CD3+CD4+ and CD3+CD8+ T lymphocytes than the PBS group, with a more pronounced increase in the combination group (Fig. 6I-L). These results indicated that the combination treatment altered the systemic immune status in tumor-bearing mice by regulating splenic immune cell composition and the proportions of peripheral blood T lymphocytes, thereby enhancing systemic anti-tumor immunity, which is related to local tumor immune microenvironment activation.

Discussion

As a typically highly vascular tumor, HCC exhibits abnormally active angiogenesis, which not only provides nutritional support for tumor proliferation but also promotes immune evasion by constructing physical barriers and an immunosuppressive microenvironment. This characteristic makes anti-angiogenic therapy one of the core strategies for systemic treatment of HCC (24). Currently, first-line multi-kinase inhibitors (MKIs) such as sorafenib and lenvatinib, as well as second-line agents such as Regorafenib and cabozantinib, exert anti-angiogenic effects by inhibiting the VEGF pathway. Moreover, combination regimens of such MKIs with immune checkpoint inhibitors (ICIs) have become a research hotspot in HCC treatment (25). However, such combination strategies face significant challenges in clinical practice: On the one hand, MKIs exhibit significant dose-dependent toxicity and dose reductions or treatment interruptions due to adverse events are extremely common, even halting the development of some ICI-anti-angiogenesis combinations (26-28); on the other hand, preclinical studies have confirmed that higher doses of MKIs may induce a hypoxic tumor microenvironment and recruit immunosuppressive cells such as TAMs, thereby exacerbating immune evasion and weakening the synergistic effect of combination therapy (11). Therefore, exploring the optimal dose of MKIs to balance efficacy, safety and immunomodulatory effects and identifying effective combination therapies are crucial for optimizing treatment regimens. The selected doses of Regorafenib (5 μg/ml *in vitro*, 5 mg/kg *in vivo*) and Nifuroxazide (10 μg/ml *in vitro*, 10 mg/kg *in vivo*) were supported by literature evidence, preliminary tests and experimental validation in the present study. For Regorafenib, the clinical recommended dose (160 mg/day) is limited by significant dose-dependent toxicity (such as hand-foot skin reactions, hypertension) (8,9,29,30). Preclinical studies consistently confirm that low doses of Regorafenib (5-10 μg/ml *in vitro*, 5-10 mg/kg/day *in vivo*) avoid systemic adverse effects while retaining key biological activities, including inhibiting VEGF-mediated angiogenesis, promoting M1 macrophage polarization and enhancing T cell infiltration, without inducing hypoxic immunosuppression (11,12). For Nifuroxazide, 10 μg/ml (*in vitro*) and 10 mg/kg/day (*in vivo*) are well-validated doses in HCC research, shown to effectively inhibit STAT3 phosphorylation, downregulate PD-L1 expression and reduce M2 macrophage infiltration in tumors (16,18). As an oral agent with decades of clinical use for gastrointestinal infections, Nifuroxazide exhibits favorable liver tissue penetration (31) and a well-documented safety profile (14). Although dedicated dose optimization procedures or full pharmacokinetic (PK) data were not collected in the present study, the selected doses are consistent with established pharmacokinetic-pharmacodynamic (PK-PD) relationships in preclinical HCC models and their rationality is directly verified by the significant anti-tumor efficacy, target inhibition and absence of toxicity in the present study. *In vivo*, this combination maintained mouse body weight and was safe. Although pharmacokinetic data were not fully collected, the doses used balanced efficacy and safety and were supported by the preclinical evidence. In addition, all drugs in the present study were administered via oral gavage, a route that closely mimics clinical oral medication. As an orally available agent with decades of clinical use, Nifuroxazide is absorbed and metabolized in the liver, with well-documented liver tissue penetration. Importantly, it has been validated as a promising anticancer candidate by inhibiting STAT3 signaling and selectively eradicating ALDH1 high cancer-initiating cells (31). Regorafenib is also clinically administered orally for advanced liver cancer treatment (7). Thus, the optimized doses and clinically relevant administration route used in the present study are directly translatable to clinical practice, jointly supporting the potential clinical application of this combination therapy. The present study is the first, to the best of the authors' knowledge, to confirm that a combination of low-dose Regorafenib and Nifuroxazide exerts a markedly enhanced anti-tumor effect in liver cancer models, with its core mechanism lying in the dual actions of targeted inhibition of the STAT3 signaling pathway and remodeling of the tumor immune microenvironment.

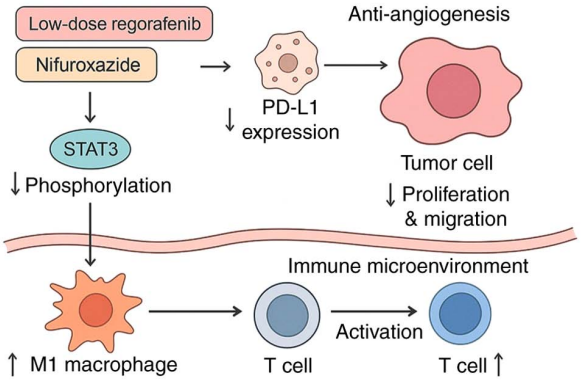

Figure 7. Proposed mechanism by which Regorafenib and Nifuroxazide exert enhanced suppression of hepatocellular carcinoma by inhibiting STAT3 and immune remodeling. Low-dose Regorafenib combined with Nifuroxazide exerts enhanced anti-tumor effects through complementary mechanisms: Nifuroxazide inhibits STAT3 phosphorylation, drives macrophage polarization toward the pro-inflammatory M1 phenotype and promotes $CD8^+$ T cell activation, thereby reversing the immunosuppressive tumor microenvironment. Concurrently, low-dose Regorafenib exerts anti-angiogenic effects by suppressing VEGF expression and downregulates PD-L1 expression on HCC cells, directly impeding tumor cell proliferation and migration. Collectively, this dual-action enhanced effect enhances immune surveillance, disrupts tumor vascular supply and amplifies the killing efficacy against HCC cells. STAT3, signal transducer and activator of transcription 3; VEGF, vascular endothelial growth factor; PD-L1, programmed death ligand 1; HCC, hepatocellular carcinoma.

Enhanced inhibition of the STAT3 pathway is the core molecular basis (32). As a key driver of tumor progression, sustained STAT3 activation can exacerbate tumor angiogenesis and immune evasion by promoting VEGF expression,

upregulating PD-L1 and recruiting immunosuppressive cells (33). The results of the present study showed that combination therapy markedly reduced p-STAT3 expression in HepG2 cells and in tumor tissues from H22 liver cancer-bearing mice. Regorafenib inhibits p-STAT3-mediated signaling by directly targeting the self-inhibited SHP-1 (34), while Nifuroxazide directly targets STAT3 phosphorylation. The two block the STAT3 pathway at different levels, jointly downregulating the expression of its downstream target genes, thereby exerting enhanced inhibition of tumor cell proliferation and migration and promoting apoptosis.

PD-L1, as a key immune checkpoint molecule, is widely expressed on the surface of tumor cells and various immune cells (35,36). Upon binding to the PD-1 receptor on T cells, it directly inhibits the activation and proliferation of effector T cells and also impairs the antigen-presenting function of macrophages in the tumor microenvironment through paracrine mechanisms (37), forming a core regulatory axis of tumor immune evasion. In HCC, abnormal activation of the PD-1/PD-L1 signaling pathway is an important pathological basis for the formation of an immunosuppressive microenvironment; blocking this pathway can relieve the functional inhibition of effector T cells and markedly enhance their specific killing of tumor cells (38). Previous studies have shown that increased T cell infiltration in tumor tissues can improve DFS (39-41). According to the results of the present study, combination therapy with low-dose Regorafenib and Nifuroxazide markedly enhanced T cell infiltration in tumor tissues and inhibited STAT3 activation, consistent with transcriptomic findings of immune pathway enrichment and further supporting its role in remodeling anti-tumor immunity. Furthermore, it was demonstrated that the combination of Regorafenib and Nifuroxazide not only markedly enhanced T cell infiltration in tumor tissues but also increased the proportion of T cells in the spleen of tumor-bearing mice.

Macrophages are closely associated with the progression of various diseases (42,43). They have become key therapeutic targets for a range of diseases, including cancer. As core effector cells of the innate immune system, macrophages exhibit high plasticity, enabling them to dynamically polarize in the TME and form a complex regulatory network with PD-L1 and VEGF (44,45). Given their pro-inflammatory phenotype, M1 macrophages can activate anti-tumor immune responses by secreting cytokines such as IFN-γ and TNF-α. M1 macrophages exhibit low surface PD-L1 expression but high levels of MHC class II molecules and co-stimulatory molecules, thereby enhancing antigen-presenting function (44,46). By contrast, M2 macrophages not only secrete large quantities of immunosuppressive cytokines, such as IL-6 and IL-10, but also bind to PD-1 on the surface of T cells through high PD-L1 expression, thereby inhibiting the activation of effector T cells and inducing the recruitment of regulatory T cells (47). Additionally, M2 macrophages release pro-angiogenic factors such as VEGF-A and MMPs and collaborate with tumor cells to form abnormal neovascular networks (48,49). This imbalance in macrophage phenotypes is particularly prominent in HCC: VEGF can hinder immune cell infiltration by promoting peritumoral collagen production and tumor angiogenesis, leading to a 'cold immune phenotype' in tumors (50,51); meanwhile, sustained activation of PD-L1 further promotes the polarization of TAMs toward the M2 phenotype (52), forming a vicious cycle of synergistic progression between immune evasion and angiogenesis. In the present study, Regorafenib and Nifuroxazide induced the polarization and recruitment of M1 macrophages in tumor tissues, while promoting the infiltration of $CD8^+$ T cells. By downregulating PD-L1 expression, the drugs relieve the inhibitory effect of TAMs on T cells, thereby establishing a positive immune cycle by promoting M1 macrophage infiltration and T cell activation.

The present study had certain limitations. First, it was based on previously used low concentrations of Regorafenib and Nifuroxazide. This concentration range may not fully cover the dose-effect relationship of the drugs under specific *in vitro* experimental conditions or *in vivo* models, potentially failing to comprehensively reflect their mechanisms of action and potential off-target effects in a broader biological context. Second, the present study relies solely on the H22 homologous model, lacking validation in xenograft models derived from human cell lines or patient-derived tissues. The H22 model was selected primarily because it retains a fully functional immune system, which is essential for investigating the immune remodeling mechanism (the core focus of the present study), but this single model may limit the generalizability and clinical translatability of the results. To address this gap, future studies will supplement two additional *in vivo* models: i) Human HCC cell line-derived xenograft (CDX) models using well-characterized human HCC cell lines (such as HepG2, Huh7) in NOD-SCID immunodeficient mice to validate direct anti-tumor effects independent of the mouse immune system; ii) Patient-derived xenograft models established from freshly isolated human HCC tissues to confirm efficacy across diverse clinical HCC subtypes. Third, the present study only used female C57BL/6 mice and the efficacy of the combination therapy in male mice remains unvalidated. The authors acknowledge restricting to female mice as a limitation; future studies will include male mice to validate efficacy across sexes. Finally, the effect of combination therapy on other immune cells was not explored in depth and the mechanism of immunomodulation remains incompletely understood. Notably, the current results only demonstrated phenotypic alterations of immune cells without functional validation. Future studies will supplement detection of immune activation markers (such as CD69, CD107a on T cells) and key functional cytokines (such as IFN-γ, TNF-α, IL-10) in tumor tissues and peripheral blood. This will further confirm whether the observed phenotypic changes translate to enhanced anti-tumor immune activity, thereby strengthening the evidence for immune remodeling mediated by the combination therapy.

In conclusion, the present study is the first, to the best of the authors' knowledge, to confirm that low-dose Regorafenib and Nifuroxazide exert significant anti-tumor effects in liver cancer models by enhancing STAT3 inhibition, downregulating PD-L1 expression, promoting M1 macrophage polarization and activating T cells. These results provided preclinical experimental evidence for the development of combined immunotherapeutic strategies for HCC.

Based on the findings of the present study, it was hypothesized that the enhanced anti-tumor effects of this combination originate from the two drugs' complementary mechanisms: Nifuroxazide inhibits STAT3 phosphorylation,

drives macrophage polarization towards the pro-inflammatory M1 phenotype and promotes $CD8^+$ T cell activation; meanwhile, low-dose Regorafenib reduces VEGF expression and downregulates PD-L1 expression in HCC cells. A schematic diagram illustrating the hypothesized molecular mechanisms of the combination treatment is shown in Fig. 7.

Acknowledgements

Not applicable.

Funding

The present study was supported by the Key Scientific Research Projects in Higher Education of Henan Province (grant no. 25A320041), the Henan Provincial Science and Technology Tackle Plan (grant no. 242102311143) and the Henan Provincial Medical Science and Technology Tackle Plan (grant no. SBCJ202103064).

Availability of data and materials

The data generated in the present study may be requested from the corresponding author.

Authors' contributions

KL and JC contributed to investigation and writing the original draft. ZZ, YG, JZ, WD, TY, XD, TZ and HJ contributed to the implementation of experiments. PC was responsible for project administration, supervision and writing the original draft. JR was responsible for conceptualization, funding acquisition, supervision and writing, reviewing and editing. All authors have read and approved the final manuscript and confirm the authenticity of all the raw data.

Ethics approval and consent to participate

All animal experiments were reviewed and approved by the Animal Ethics Committee of the First Affiliated Hospital of Zhengzhou University (approval no. 2023-KY-1333). This committee operates independently, free from undue influence by researchers or sponsors and is duly qualified to oversee animal research ethics. All experiments were conducted in strict compliance with the General Requirements for Biosafety in Animal Experiments of Laboratory Animals in China (GB/T 43051-2023) (53), which is consistent with internationally recognized animal welfare guidelines, including the basic principles outlined in the National Institutes of Health Guide for the Care and Use of Laboratory Animals. Every effort was made to minimize animal suffering and ensure animal welfare.

Patient consent for publication

Not applicable.

Competing interests

The authors declare that they have no competing interests.

References

1. Anwanwan D, Singh SK, Singh S, Saikam V and Singh R: Challenges in liver cancer and possible treatment approaches. Biochim Biophys Acta Rev Cancer 1873: 188314, 2020.
2. Rumgay H, Arnold M, Ferlay J, Lesi O, Cabasag CJ, Vignat J, Laversanne M, McGlynn KA and Soerjomataram I: Global burden of primary liver cancer in 2020 and predictions to 2040. J Hepatol 77: 1598-1606, 2022.
3. Marrero JA, Kulik LM, Sirlin CB, Zhu AX, Finn RS, Abecassis MM, Roberts LR and Heimbach JK: Diagnosis, staging and management of hepatocellular carcinoma: 2018 practice guidance by the american association for the study of liver diseases. Hepatology 68: 723-750, 2018.
4. Brown ZJ, Tsilimigras DI, Ruff SM, Mohseni A, Kamel IR, Cloyd JM and Pawlik TM: Management of hepatocellular carcinoma: A review. JAMA Surg 158: 410-420, 2023.
5. Kudo M: Targeted and immune therapies for hepatocellular carcinoma: Predictions for 2019 and beyond. World J Gastroenterol 25: 789-807, 2019.
6. Guo X, Zhao Z, Zhu L, Liu S, Zhou L, Wu F, Fang S, Chen M, Zheng L and Ji J: The evolving landscape of biomarkers for systemic therapy in advanced hepatocellular carcinoma. Biomark Res 13: 60, 2025.
7. Demols A, Borbath I, Van den Eynde M, Houbiers G, Peeters M, Marechal R, Delaunoit T, Goemine JC, Laurent S, Holbrechts S, *et al*: Regorafenib after failure of gemcitabine and platinum-based chemotherapy for locally advanced/metastatic biliary tumors: REACHIN, a randomized, double-blind, phase II trial. Ann Oncol 31: 1169-1177, 2020.
8. Bruix J, Qin S, Merle P, Granito A, Huang YH, Bodoky G, Pracht M, Yokosuka O, Rosmorduc O, Breder V, *et al*: Regorafenib for patients with hepatocellular carcinoma who progressed on sorafenib treatment (RESORCE): A randomised, double-blind, placebo-controlled, phase 3 trial. Lancet 389: 56-66, 2017.
9. Grothey A, Van Cutsem E, Sobrero A, Siena S, Falcone A, Ychou M, Humblet Y, Bouché O, Mineur L, Barone C, *et al*: Regorafenib monotherapy for previously treated metastatic colorectal cancer (CORRECT): An international, multicentre, randomised, placebo-controlled, phase 3 trial. Lancet 381: 303-312, 2013.
10. Ou DL, Chen CW, Hsu CL, Chung CH, Feng ZR, Lee BS, Cheng AL, Yang MH and Hsu C: Regorafenib enhances antitumor immunity via inhibition of p38 kinase/Creb1/Klf4 axis in tumor-associated macrophages. J Immunother Cancer 9: e001657, 2021.
11. Lin YY, Tan CT, Chen CW, Ou DL, Cheng AL and Hsu C: Immunomodulatory effects of current targeted therapies on hepatocellular carcinoma: Implication for the future of immunotherapy. Semin Liver Dis 38: 379-388, 2018.
12. Bajpai P, Agarwal S, Afaq F, Al Diffalha S, Chandrashekar DS, Kim HG, Shelton A, Miller CR, Singh SK, Singh R, *et al*: Combination of dual JAK/HDAC inhibitor with regorafenib synergistically reduces tumor growth, metastasis and regorafenib-induced toxicity in colorectal cancer. J Exp Clin Cancer Res 43: 192, 2024.
13. Al Zaid Siddiquee K and Turkson J: STAT3 as a target for inducing apoptosis in solid and hematological tumors. Cell Res 18: 254-267, 2008.
14. Begovic B, Ahmedtagic S, Calkic L, Vehabović M, Kovacevic SB, Catic T and Mehic M: Open Clinical trial on using nifuroxazide compared to probiotics in treating acute diarrhoeas in adults. Mater Sociomed 28: 454-458, 2016.
15. Luo L, Xu F, Peng H, Luo Y, Tian X, Battaglia G, Zhang H, Gong Q, Gu Z and Luo K: Stimuli-responsive polymeric prodrug-based nanomedicine delivering nifuroxazide and doxorubicin against primary breast cancer and pulmonary metastasis. J Control Release 318: 124-135, 2020.
16. Zhao T, Wei P, Zhang C, Zhou S, Liang L, Guo S, Yin Z, Cheng S, Gan Z, Xia Y, *et al*: Nifuroxazide suppresses PD-L1 expression and enhances the efficacy of radiotherapy in hepatocellular carcinoma. Elife 12: RP90911, 2024.
17. Chen P, Li K, Chen J, Hei H, Geng J, Huang N, Lei M, Jia H, Ren J and Jin C: Enhanced effect of radiofrequency ablation on HCC by siRNA-PD-L1-endostatin Co-expression plasmid delivered. Transl Oncol 53: 102319, 2025.
18. Ye TH, Yang FF, Zhu YX, Li YL, Lei Q, Song XJ, Xia Y, Xiong Y, Zhang LD, Wang NY, *et al*: Inhibition of STAT3 signaling pathway by nifuroxazide improves antitumor immunity and impairs colorectal carcinoma metastasis. Cell Death Dis 8: e2534, 2017.

19. Aden DP, Fogel A, Plotkin S, Damjanov I and Knowles BB: Controlled synthesis of HBsAg in a differentiated human liver carcinoma-derived cell line. Nature 282: 615-616, 1979.
20. Knowles BB, Howe CC and Aden DP: Human hepatocellular carcinoma cell lines secrete the major plasma proteins and hepatitis B surface antigen. Science 209: 497-499, 1980.
21. López-Terrada D, Cheung SW, Finegold MJ and Knowles BB: Hep G2 is a hepatoblastoma-derived cell line. Hum Pathol 40: 1512-1515, 2009.
22. de Souza GO, Wasinski F and Donato J: Characterization of the metabolic differences between male and female C57BL/6 mice. Life Sci 301: 120636, 2022.
23. Subramanian A, Tamayo P, Mootha VK, Mukherjee S, Ebert BL, Gillette MA, Paulovich A, Pomeroy SL, Golub TR, Lander ES and Mesirov JP: Gene set enrichment analysis: A knowledge-based approach for interpreting genome-wide expression profiles. Proc Natl Acad Sci USA 102: 15545-15550, 2005.
24. Poon RTP, Fan ST and Wong J: Clinical significance of angiogenesis in gastrointestinal cancers: A target for novel prognostic and therapeutic approaches. Ann Surg 238: 9-28, 2003.
25. Cheng AL, Hsu C, Chan SL, Choo SP and Kudo M: Challenges of combination therapy with immune checkpoint inhibitors for hepatocellular carcinoma. J Hepatol 72: 307-319, 2020.
26. Amin A, Plimack ER, Ernstoff MS, Lewis LD, Bauer TM, McDermott DF, Carducci M, Kollmannsberger C, Rini BI, Heng DYC, *et al*: Safety and efficacy of nivolumab in combination with sunitinib or pazopanib in advanced or metastatic renal cell carcinoma: The CheckMate 016 study. J Immunother Cancer 6: 109, 2018.
27. Xu J, Zhang Y, Jia R, Yue C, Chang L, Liu R, Zhang G, Zhao C, Zhang Y, Chen C, *et al*: Anti-PD-1 antibody SHR-1210 combined with apatinib for advanced hepatocellular carcinoma, gastric, or esophagogastric junction cancer: An open-label, dose escalation and expansion study. Clin Cancer Res 25: 515-523, 2019.
28. Finn RS, Ikeda M, Zhu AX, Sung MW, Baron AD, Kudo M, Okusaka T, Kobayashi M, Kumada H, Kaneko S, *et al*: Phase Ib study of lenvatinib plus pembrolizumab in patients with unresectable hepatocellular carcinoma. J Clin Oncol 38: 2960-2970, 2020.
29. Killock D: Liver cancer: Regorafenib-a new RESORCE in HCC. Nat Rev Clin Oncol 14: 70-71, 2016.
30. Hecht JR, Park YS, Tabernero J, Lee MA, Lee S, Virgili AC, Van den Eynde M, Fontana E, Fakih M, Asghari G, *et al*: Zanzalintinib plus atezolizumab versus regorafenib in refractory colorectal cancer (STELLAR-303): A randomised, open-label, phase 3 trial. Lancet 406: 2360-2370, 2025.
31. Bailly C: Toward a repositioning of the antibacterial drug nifuroxazide for cancer treatment. Drug Discov Today 24: 1930-1936, 2019.
32. Hu B, Zou T, Qin W, Shen X, Su Y, Li J, Chen Y, Zhang Z, Sun H, Zheng Y, *et al*: Inhibition of EGFR overcomes acquired lenvatinib resistance driven by STAT3-ABCB1 signaling in hepatocellular carcinoma. Cancer Res 82: 3845-3857, 2022.
33. Zou S, Tong Q, Liu B, Huang W, Tian Y and Fu X: Targeting STAT3 in cancer immunotherapy. Mol Cancer 19: 145, 2020.
34. Tai WT, Chu PY, Shiau CW, Chen YL, Li YS, Hung MH, Chen LJ, Chen PL, Su JC, Lin PY, *et al*: STAT3 mediates regorafenib-induced apoptosis in hepatocellular carcinoma. Clin Cancer Res 20: 5768-5776, 2014.
35. Voli F, Valli E, Lerra L, Kimpton K, Saletta F, Giorgi FM, Mercatelli D, Rouaen JRC, Shen S, Murray JE, *et al*: Intratumoral copper modulates PD-L1 expression and influences tumor immune evasion. Cancer Res 80: 4129-4144, 2020.
36. Wang X, Yang X, Zhang C, Wang Y, Cheng T, Duan L, Tong Z, Tan S, Zhang H, Saw PE, *et al*: Tumor cell-intrinsic PD-1 receptor is a tumor suppressor and mediates resistance to PD-1 blockade therapy. Proc Natl Acad Sci USA 117: 6640-6650, 2020.
37. Xiong H, Mittman S, Rodriguez R, Moskalenko M, Pacheco-Sanchez P, Yang Y, Nickles D and Cubas R: Anti-PD-L1 treatment results in functional remodeling of the macrophage compartment. Cancer Res 79: 1493-1506, 2019.
38. Tabrizian P, Abdelrahim M and Schwartz M: Immunotherapy and transplantation for hepatocellular carcinoma. J Hepatol 80: 822-825, 2024.
39. Wu TD, Madireddi S, de Almeida PE, Banchereau R, Chen YJ, Chitre AS, Chiang EY, Iftikhar H, O'Gorman WE, Au-Yeung A, *et al*: Peripheral T cell expansion predicts tumour infiltration and clinical response. Nature 579: 274-278, 2020.
40. Sun L, Su Y, Jiao A, Wang X and Zhang B: T cells in health and disease. Signal Transduct Target Ther 8: 235, 2023.
41. Fridman WH, Pagès F, Sautès-Fridman C and Galon J: The immune contexture in human tumours: Impact on clinical outcome. Nat Rev Cancer 12: 298-306, 2012.
42. Varol C, Mildner A and Jung S: Macrophages: Development and tissue specialization. Annu Rev Immunol 33: 643-675, 2015.
43. Lavin Y, Mortha A, Rahman A and Merad M: Regulation of macrophage development and function in peripheral tissues. Nat Rev Immunol 15: 731-744, 2015.
44. Sharma A, Seow JJW, Dutertre CA, Pai R, Blériot C, Mishra A, Wong RMM, Singh GSN, Sudhagar S, Khalilnezhad S, *et al*: Onco-fetal reprogramming of endothelial cells drives immunosuppressive macrophages in hepatocellular carcinoma. Cell 183: 377-394.e21, 2020.
45. Lu LG, Zhou ZL, Wang XY, Liu BY, Lu JY, Liu S, Zhang GB, Zhan MX and Chen Y: PD-L1 blockade liberates intrinsic antitumourigenic properties of glycolytic macrophages in hepatocellular carcinoma. Gut 71: 2551-2560, 2022.
46. Cheng K, Cai N, Zhu J, Yang X, Liang H and Zhang W: Tumor-associated macrophages in liver cancer: From mechanisms to therapy. Cancer Commun (Lond) 42: 1112-1140, 2022.
47. Locati M, Curtale G and Mantovani A: Diversity, mechanisms and significance of macrophage plasticity. Annu Rev Pathol 15: 123-147, 2020.
48. Yeung OW, Lo CM, Ling CC, Qi X, Geng W, Li CX, Ng KT, Forbes SJ, Guan XY, Poon RT, *et al*: Alternatively activated (M2) macrophages promote tumour growth and invasiveness in hepatocellular carcinoma. J Hepatol 62: 607-616, 2015.
49. Kadioglu E and De Palma M: Cancer metastasis: Perivascular macrophages under watch. Cancer Discov 5: 906-908, 2015.
50. Gabrilovich DI, Chen HL, Girgis KR, Cunningham HT, Meny GM, Nadaf S, Kavanaugh D and Carbone DP: Production of vascular endothelial growth factor by human tumors inhibits the functional maturation of dendritic cells. Nat Med 2: 1096-1103, 1996.
51. Rahma OE and Hodi FS: The intersection between tumor angiogenesis and immune suppression. Clin Cancer Res 25: 5449-5457, 2019.
52. Zhang H, Liu L, Liu J, Dang P, Hu S, Yuan W, Sun Z, Liu Y and Wang C: Roles of tumor-associated macrophages in anti-PD-1/PD-L1 immunotherapy for solid cancers. Mol Cancer 22: 58, 2023.
53. National Standard of the People's Republic of China: Laboratory animal - General requirements for biosafety in animal experiment (GB/T 43051-2023) [S]. National Standard of the People's Republic of China, Beijing, 2023.